Supplementary material

An innovative approach to measuring hygroscopic scattering enhancement using a humidified single-nephelometer system

Lenka Suchánková[1,2,3], Jakub Ondráček[1], Naděžda Zíková[1], Petr Roztočil[1], Petr Vodička[1], Roman Prokeš[2,3], Ivan Holoubek[2,3+], Vladimír Ždímal[1]

[1]Institute of Chemical Process Fundamentals of the Czech Academy of Sciences, Prague, 165 00, Czech Republic
[2]Global Change Research Institute of the Czech Academy of Sciences, Brno, 603 00, Czech Republic
[3]RECETOX, Faculty of Science, Masaryk University, Brno, 611 37, Czech Republic
[+] deceased

Correspondence to: Lenka Suchánková (suchankova@icpf.cas.cz)

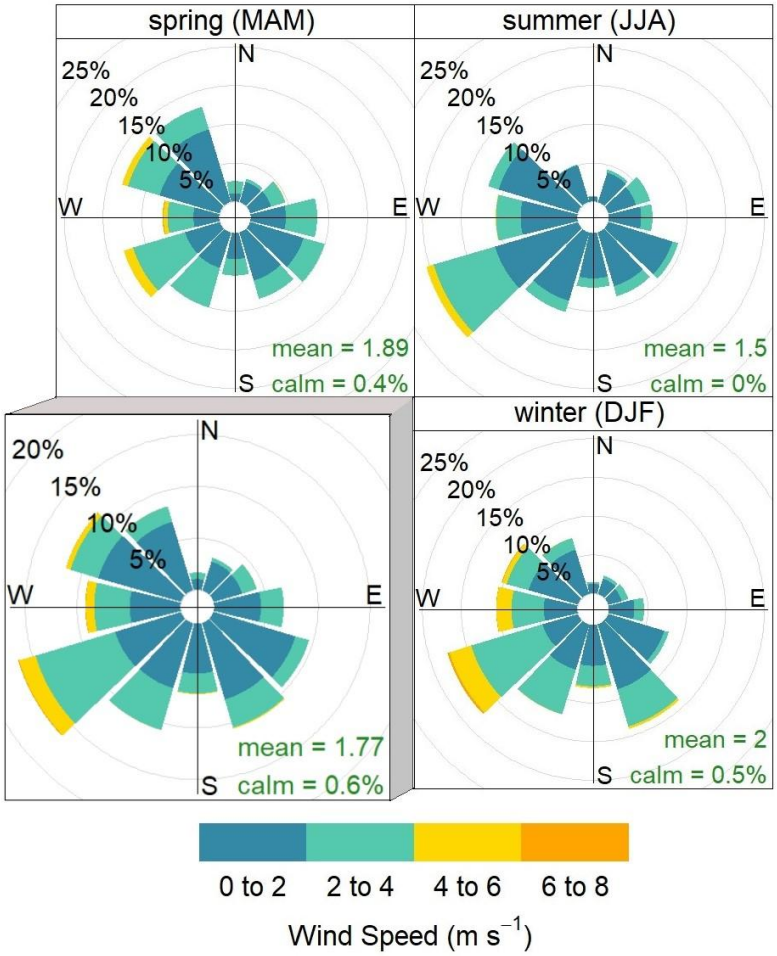

Figure S.1: The frequency of counts by wind direction from November 2022 to August 2023 (see bottom left) and wind directions by seasons alongside the mean wind speed and percentage of calm days (0 ms^{-1}). It should be noted that the fall season is not presented due to an insufficient amount of data.

Table S.1: Overall and seasonal data availability expressed as f(RH) and $f(RH)_{bsp}$ data points (%) at 450, 550, and 700 nm (November 2022 – August 2023).*

	f(RH)			$f(RH)_{bsp}$		
	450 nm	**550 nm**	**700 nm**	**450 nm**	**550 nm**	**700 nm**
Whole period	5145 (77 %)	5145 (77 %)	5145 (77 %)	5134 (77 %)	5142 (77 %)	5143 (77 %)
Fall	366 (96 %)	366 (96 %)	366 (96 %)	366 (96 %)	366 (96 %)	366 (96 %)
Winter	1478 (68 %)	1478 (68 %)	1478 (68 %)	1477 (68 %)	1477 (68 %)	1477 (68 %)
Spring	1741 (79 %)	1741 (79 %)	1741 (79 %)	1739 (79 %)	1739 (79 %)	1740 (79 %)
Summer	1560 (81 %)	1560 (81 %)	1560 (81 %)	1552 (81 %)	1560 (81 %)	1560 (81 %)

* Data availability was calculated as the percentage of actual hourly measurements compared to the total possible hourly measurements within each season during the campaign period.

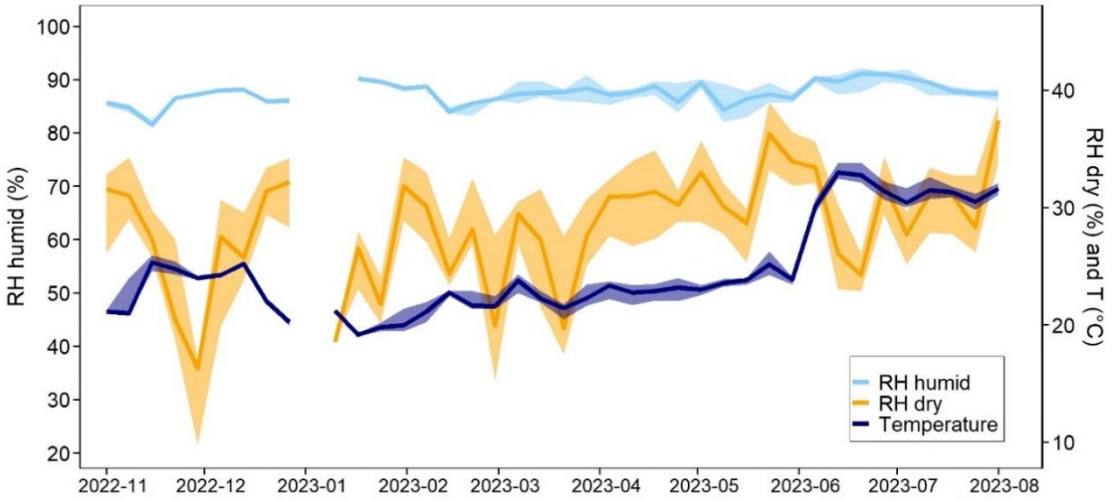

Figure S.2: Variability of RH in humidified (RH humid) and dry (RH dry) mode and temperature in dry mode over the study period. Solid lines represent weekly median variation, and shaded areas 25th and 75th percentiles.

Table S.2: The RH (%) and T (K) statistics in the cell during humidified and dry modes. P10, P25, P50, P75, and P90 denote respective percentiles.

	Humidified mode		**Dry mode**	
	RH_{cell} (%)	**T_{cell} (K)**	**RH_{cell} (%)**	**T_{cell} (K)**
Mean ± sd	87.34 ± 2.67	297.91 ± 4.15	28.36 ± 5.85	297.94 ± 4.16
P10	83.62	293.57	20.30	293.46
P25	85.81	295.01	25.05	294.92
P50	87.64	296.83	28.84	296.77
P75	89.31	299.13	32.43	299.29
P90	90.50	304.94	35.34	304.93

Table S.3: Slopes, intercepts, and R^2 retrieved from the weighted bivariate fit of $f(RH)_{bsp}$ vs. the f(RH) at λ = 550 nm. Values in brackets characterize respective uncertainties.

	Slope			**Intercept**			**R^2**		
	450 nm	**550 nm**	**700 nm**	**450 nm**	**550 nm**	**700 nm**	**450 nm**	**550 nm**	**700 nm**
Whole	0.755 (0.008)	0.633 (0.003)	0.502 (0.005)	0.248 (0.011)	0.285 (0.005)	0.414 (0.008)	0.64	0.88	0.72
Fall	0.681 (0.016)	0.453 (0.007)	0.779 (0.017)	0.385 (0.022)	0.527 (0.009)	-0.028 (0,030)	0.84	0.93	0.85
Winter	0.850 (0.014)	0.723 (0.004)	0.511 (0.007)	0.131 (0.019)	0.172 (0.006)	0.397 (0.013)	0.71	0.95	0.77
Spring	0.751 (0.013)	0.661 (0.006)	0.440 (0.007)	0.264 (0.019)	0.257 (0.008)	0.537 (0.013)	0.65	0.89	0.68
Summer	0.720 (0.021)	0.673 (0.007)	0.431 (0.007)	0.265 (0.029)	0.207 (0.010)	0.519 (0.013)	0.44	0.84	0.70

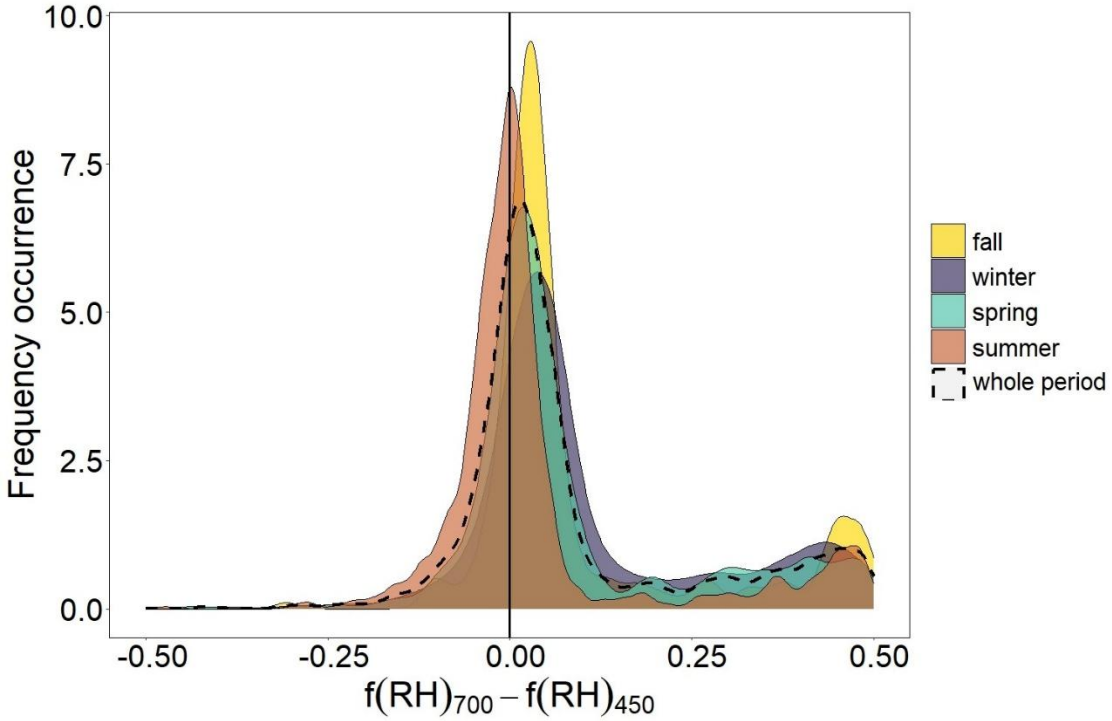

Figure S.3: Frequency occurrence of f(RH) measured at 700 and 450 nm for the whole measurement campaign and the individual seasons.

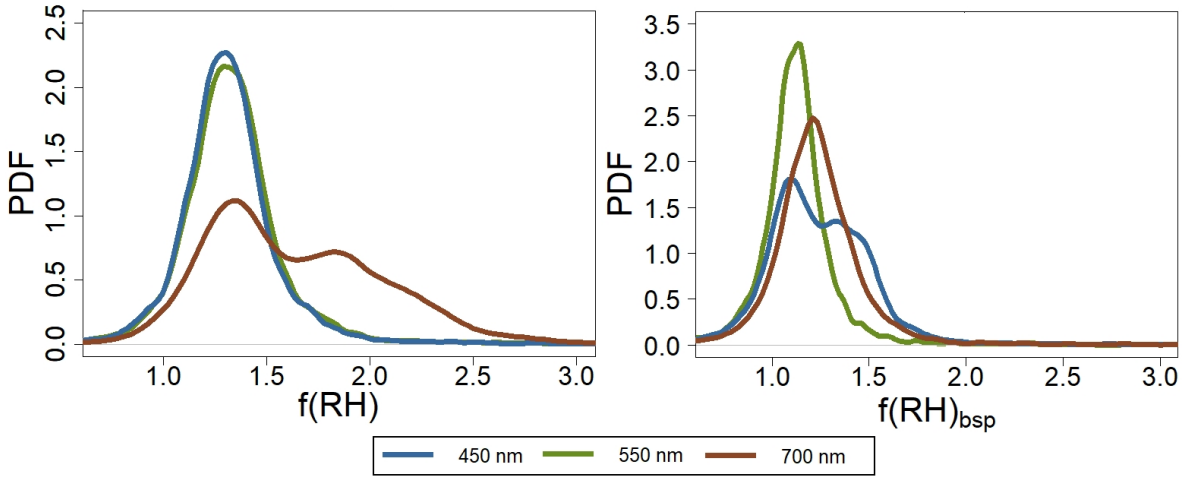

Figure S.4: The probability density functions (PDF) of the f(RH) (left) and the $f(RH)_{bsp}$ (right) at 450, 550, and 700 nm for the whole measuring campaign (November 2022 – August 2023).

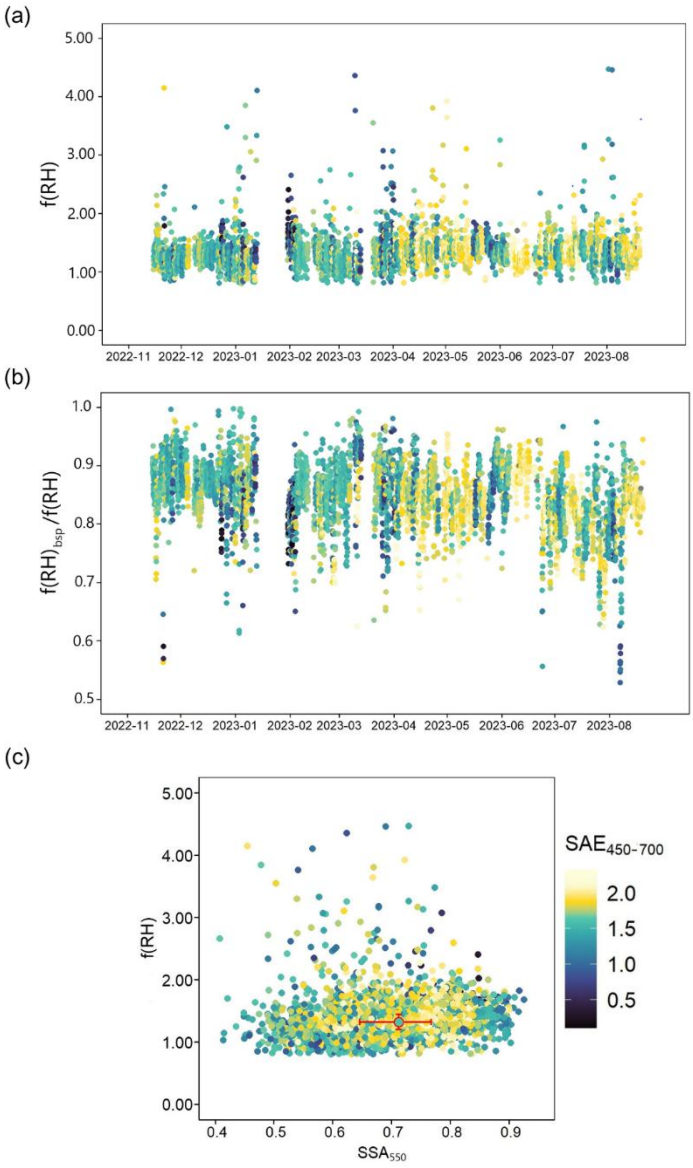

Figure S.5: Temporal variation of f(RH) (a) and the ratio of $f(RH)_{bsp}$ and f(RH) (b) at 550 nm, color-coded with a dry $SAE_{450-700}$. Scatterplot of the f(RH) at 550 nm vs SSA_{550} during the campaign, color-coded with median $SAE_{450-700}$ (c). The red circle with red error bars estimated the median point with interquartile ranges.

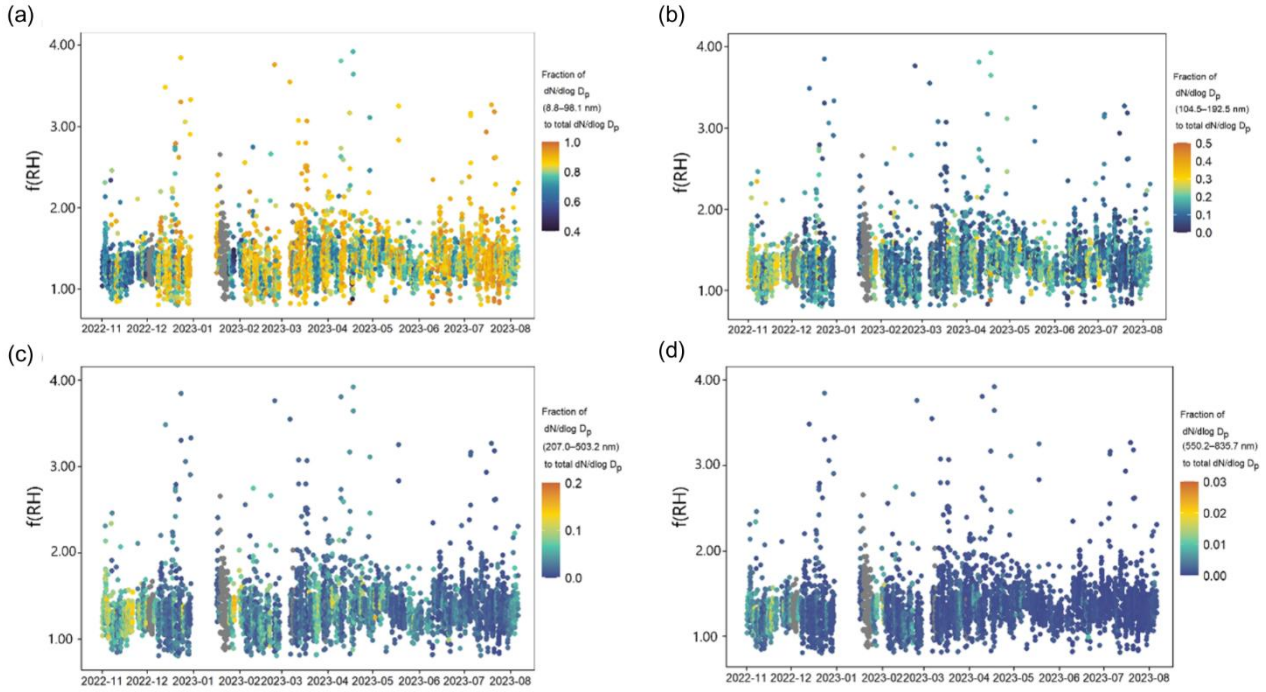

Figure S.6: Temporal variation of f(RH) at 550 nm color-coded with the fraction of the size selected dN/dlog D_p to the overall dN/dlog D_p. 8.8 nm < D_p < 98.1 nm (a), 104.5 nm < D_p < 192.5 nm (b), 207.0 nm < D_p < 503.2 nm (c), and 550.2 nm < D_p < 835.7 nm (d). It should be noted that the fractions of the respective size modes have different scales for better readability. The gray points represent missing PNSD measurements.

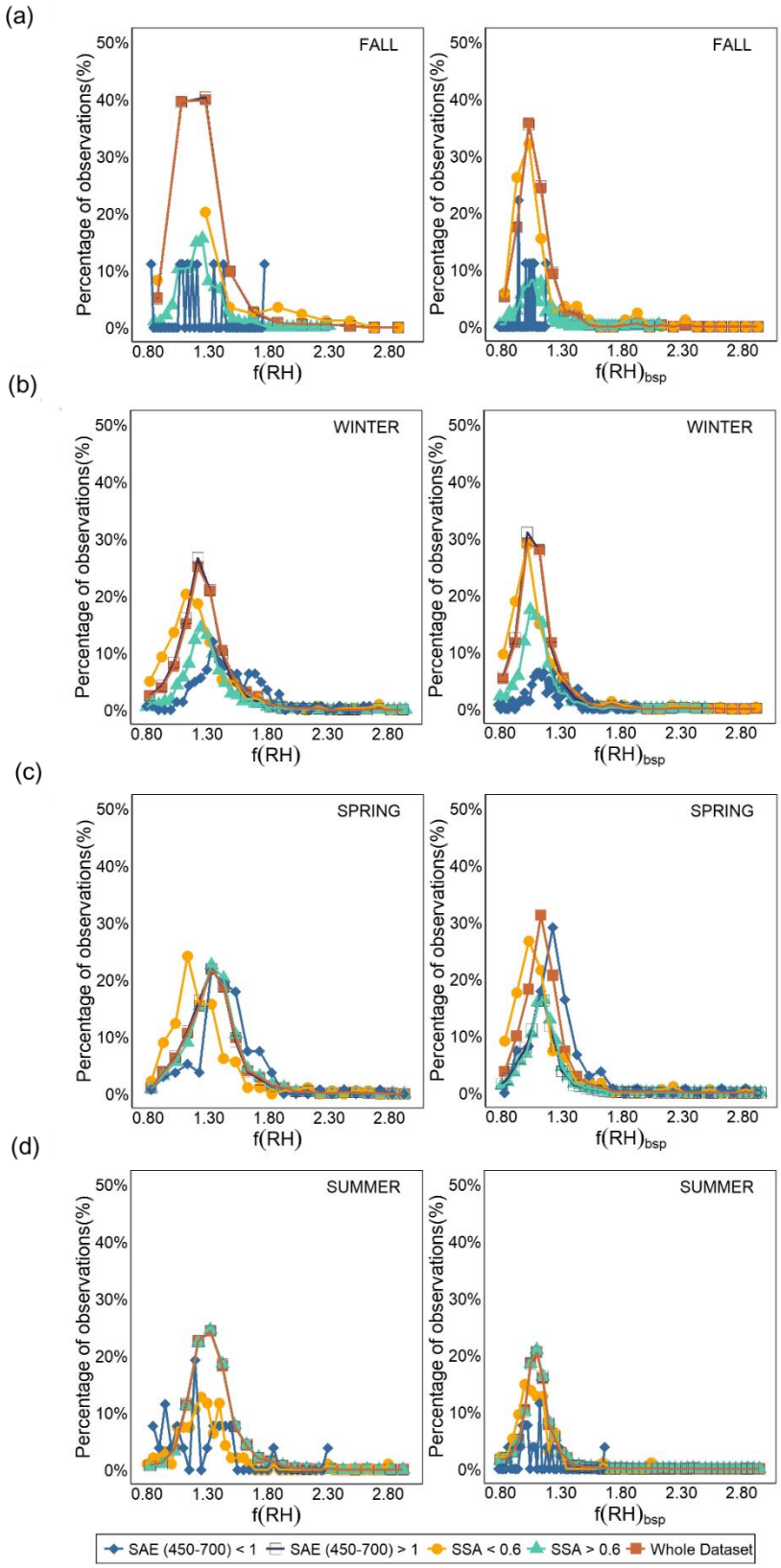

Figure S.7: Frequency distribution of f(RH) (left) and $f(RH)_{bsp}$ (right) at 550 nm during fall (a), winter (b), spring (c), and summer (d), color and symbol-coded based on $SAE_{450\text{-}700}$ and SSA_{550}.

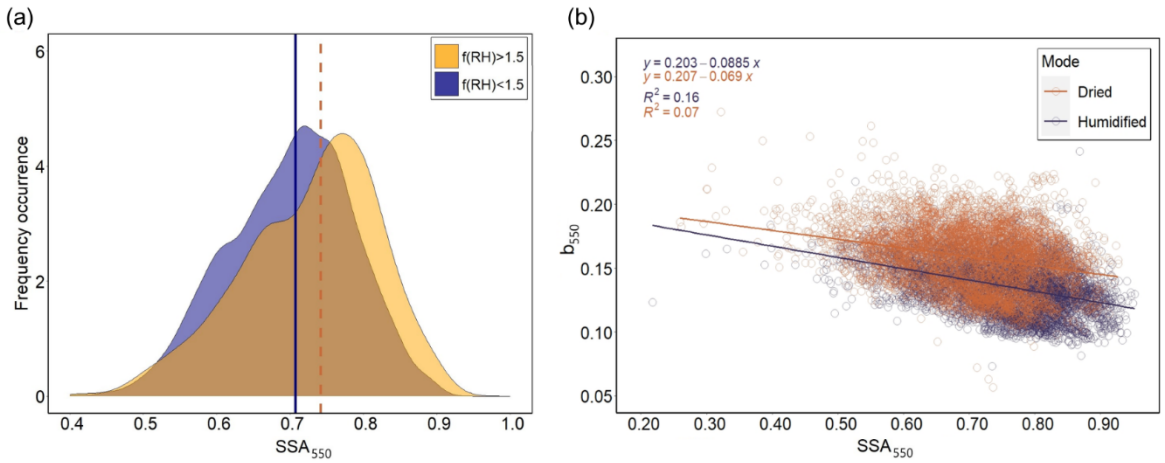

Figure S.8: Frequency distribution of dry SSA_{550} for f(RH) > 1.5 (ochre) and f(RH) < 1.5 (purple) with respective median values (vertical solid purple line for f(RH) < 1.5 and vertical dashed line for f(RH) < 1.5 represents median value of SSA_{550} for f(RH) > 1.5, respectively) (a). Relationship between b_{550} and SSA_{550} at dried (orange) and humidified (purple) conditions (b).

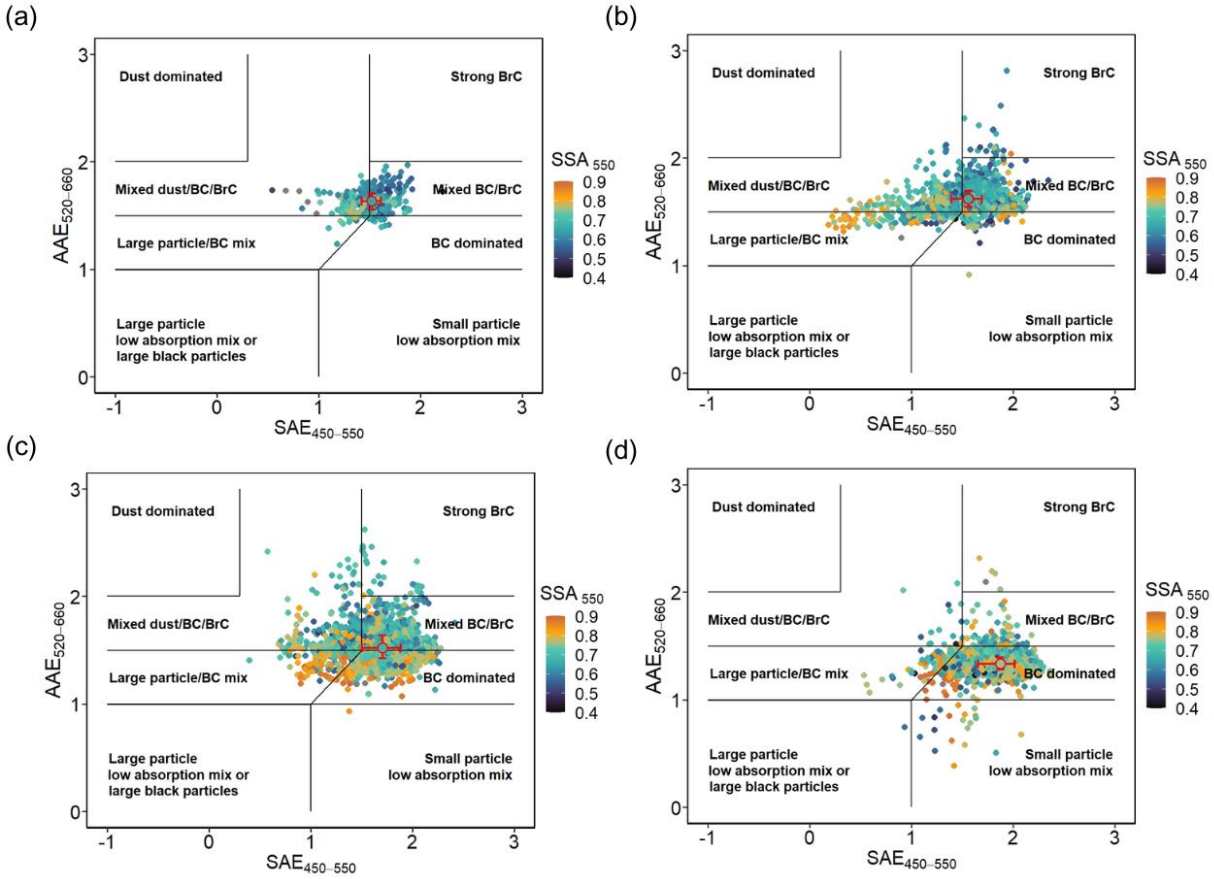

Figure S.9: $AAE_{520\text{-}660}$ vs. $SAE_{450\text{-}550}$ hourly means color-coded with SSA_{550} with the aerosol characterization matrix for fall (a), winter (b), spring (c), and summer (d) adopted from Cappa et al. (2016) and Cazorla et al. (2013). The red circle with red error bars estimated the median $AAE_{520\text{-}660}$-$SAE_{450\text{-}550}$ point with interquartile ranges. The color of the circle is color-coded based on the median of SSA_{550}.

Table S.4: Spearman correlation coefficients between f(RH) and $f(RH)_{bsp}$ at 550 nm and the concentration of total carbon (TC), organic carbon (OC), elemental carbon (EC), primary organic carbon (POC), secondary organic carbon (SOC), the ratio of SOC and OC, the ratio or more volatile OC fractions (OC1+OC2) to less volatile OC fractions (OC3+OC4) and the ratio of OC and EC for whole period and individual seasons. Bold coefficients are significant at p < 0.0001.

	Spearman correlation coefficients R					
		f(RH)	$f(RH)_{bsp}$		f(RH)	$f(RH)_{bsp}$
TC	**Whole**	**-0.30**	**-0.13**	OC	**Whole**	**-0.28**	**-0.12**
	Fall	**-0.38**	-0.15		**Fall**	**-0.38**	-0.16
	Winter	**-0.33**	< 0.01		**Winter**	**-0.22**	< 0.01
	Spring	**-0.25**	**-0.12**		**Spring**	**-0.23**	< 0.01
	Summer	**-0.33**	**-0.17**		**Summer**	**-0.32**	**-0.18**
EC	**Whole**	**-0.33**	**-0.17**	POC	**Whole**	**-0.33**	**-0.17**
	Fall	**-0.36**	-0.11		**Fall**	**-0.36**	-0.11
	Winter	**-0.20**	< 0.01		**Winter**	**-0.20**	< 0.01
	Spring	**-0.30**	**-0.24**		**Spring**	**-0.31**	**-0.24**
	Summer	**-0.30**	**-0.12**		**Summer**	**-0.30**	**-0.12**
SOC	**Whole**	**-0.20**	< 0.01	SOC/OC	**Whole**	**0.29**	**0.17**
	Fall	**-0.30**	-0.13		**Fall**	0.14	< 0.01
	Winter	**-0.22**	< 0.01		**Winter**	**0.17**	< 0.01
	Spring	**-0.13**	< 0.01		**Spring**	**0.31**	**0.30**
	Summer	**-0.28**	**-0.17**		**Summer**	**0.21**	< 0.01
OC1+OC2/OC3+OC4	**Whole**	**0.30**	**0.18**	OC/EC	**Whole**	**0.29**	**0.17**
	Fall	0.02	< 0.01		**Fall**	0.14	< 0.01
	Winter	**0.21**	**0.12**		**Winter**	**0.17**	< 0.01
	Spring	**0.43**	**0.28**		**Spring**	**0.31**	0.30
	Summer	**0.22**	**0.16**		**Summer**	**0.19**	< 0.01
OC/TC	**Whole**	**0.29**	**0.17**				
	Fall	0.16	< 0.01				
	Winter	**0.17**	< 0.01				
	Spring	**0.32**	**0.30**				
	Summer	**0.19**	< 0.01				

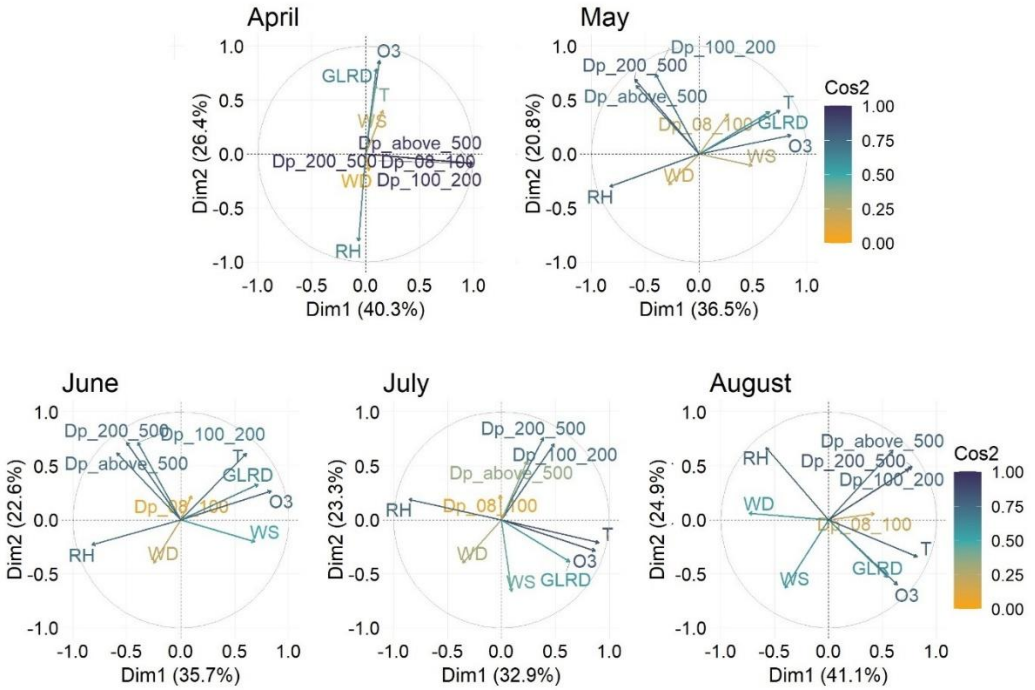

Figure S.10: Principal component analysis (PCA) results for April to July, based on the number concentrations of different particle size modes (Dp_8_100, Dp_100_200, Dp_200_500, and Dp_above_500; where, e.g., Dp_8_100 represents the number concentration of particles between 8 and 100 nm) and NPF-related environmental parameters (T = temperature, O_3 = ozone concentration, RH = relative humidity, GLRD = global radiation, WD = wind direction, WS = wind speed). Each PCA was conducted individually for each month. Arrows represent variable contributions. The squared cosine (Cos^2) values indicate the quality of representation of each variable on the first two principal components (Dim1 and Dim2); variables with higher Cos^2 values are better represented in the current PCA space.

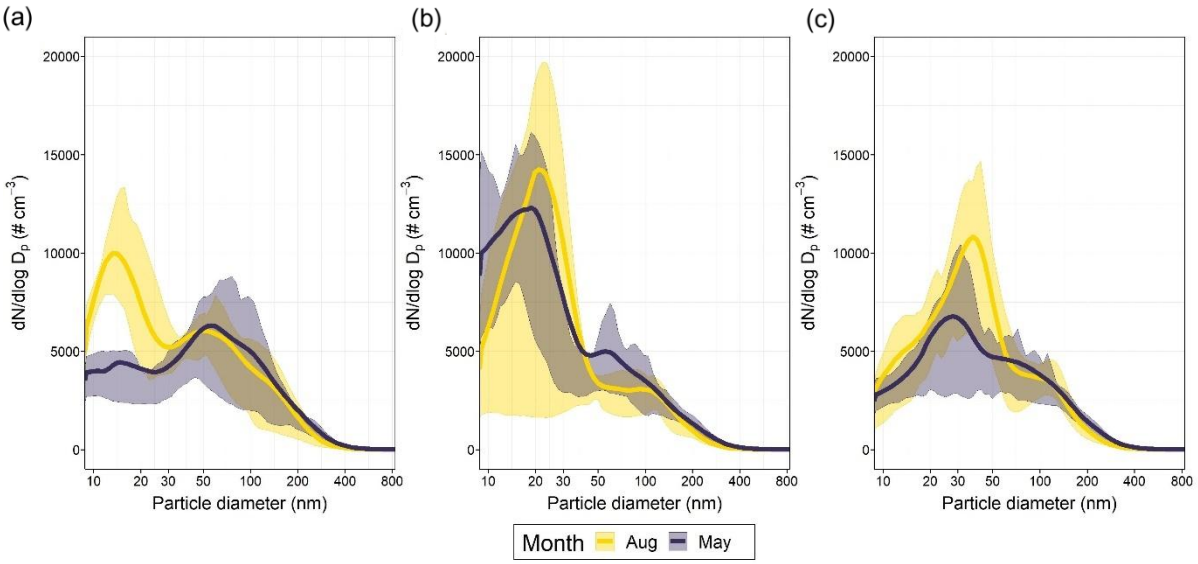

Figure S.11: The particle size number distributions (dN/dlog D_p) during days identified with NPF events in May and August at 6:30-8:30 AM UTC (a), 11:30 AM-1:30 PM UTC (b), and 4:30-6:30 PM UTC (c).